Available online at www.sciencedirect.com
ScienceDirect
Scripta Materialia 57 (2007) 409–412
Scripta MATERIALIA
www.elsevier.com/locate/scriptamat

Fatigue response of NiFeGa single crystals

Christos Efstathiou,[a] Huseyin Sehitoglu,[a,*] Peter Kurath,[a] Stefano Foletti[b] and Piermaria Davoli[b]

[a] *Department of Mechanical Science and Engineering, University of Illinois, 1206 W. Green St., Urbana, IL 61801, USA*
[b] *Department of Mechanical Engineering, Politecnico di Milano, Via La Masa 34, 20156 Milano, Italy*

Received 27 March 2007; accepted 30 April 2007

The tensile fatigue response of single crystal NiFeGa with [0 0 1], [0 1 1] and [1 2 3] orientations was investigated under pseudoelastic conditions. The [0 0 1] orientation displayed a remarkably long fatigue life, exceeding 13,000 cycles, when loaded to a 10% strain range. The [1 2 3] orientation displayed the shortest fatigue life and the [0 1 1] intermediate. Although the fatigue lives drastically varied for all three orientations, the stabilization of the stress–strain curves was similar. The lack of residual strains and the stability of the stress–strain curves indicate excellent fatigue resistance.

Keywords: Fatigue; Cyclic stability; Fatigue life; Pseudoelasticity

Shape memory alloys (SMAs) experience cyclic loading in actuation, sensing and biomedical applications. These applications often exploit the large pseudoelastic deformation properties of SMAs. Emerging applications demand large cyclic strains (>5%) without loss of recoverability. Although NiTi alloys are most widely used, at fully reversed strains of ±5% their fatigue lives are <1000 cycles [1]. The CuNiAl alloys exhibit better fatigue resistance with lives of 3000 cycles under a tensile strain range of 10% [2]. The quest for new materials with high fatigue resistance, large pseudoelastic capability and long fatigue life is an ongoing effort, and the current investigation is focused on this need.

Recently developed NiFeGa SMAs are promising ferromagnetic actuating and sensing materials. The temperature dependence of the tensile and compressive response has been reported for $Ni_{54}Fe_{19}Ga_{27}$ (at.%) [3–5]. Large, fully recoverable tensile strains greater than 10% have been measured in selective single crystal orientations [4,5]. Experimental and theoretical transformation strains for NiFeGa exceed that for NiTi and most other commercial SMAs. NiFeGa also displays complete pseudoelastic recovery over a wider temperature range (>300 °C) than has been observed for other SMAs [5]. However, the fatigue resistance or the cyclic stability of the stress–strain curve has not been reported for NiFeGa.

To characterize the deformation response and in turn the fatigue resistance we define the relevant material parameters in Figure 1. For crystal orientations near the [0 0 1] pole of the stereographic triangle, a two-stage transformation in NiFeGa is observed in tension [4,5]. Based on our work (including extensive strain-temperature experiments [5]) we identified the "first" as $A \rightarrow 10M \rightarrow 14M$ and the "second" transformation as $14M \rightarrow L10$. We refer to cubic austenite with $L21$ atomic order as A, the martensite phases as 10M or 14M (describing 5 and 7 modulation periods), and the unmodulated tetragonal lattice as $L10$. The "first" transformation will be referred to as SIM1 and the "second" transition as SIM2 (where SIM refers to stress-induced martensite). The critical stress (σ_{cr}) for SIM1 is defined at the onset of the transition in Figure 1. The transformation strain (ε_{tr}) for SIM1 is also shown in Figure 1. The stress hysteresis ($\Delta\sigma$) is defined at half the ε_{tr} in Figure 1 for SIM1 and SIM2 respectively. In addition, the applied strain range ($\Delta\varepsilon$) is shown in Figure 1. Previous works on other SMAs have found the change in these material parameters to be dependent on test temperature [6,7], alloy composition [8], crystal orientation [9–12] and test control parameters [13]. Specifically, some researchers have cycled between fixed stress limits [1,13], whereas others have enforced either a fixed strain range [1,9,11,14,15] or a constant

* Corresponding author. E-mail: huseyin@uiuc.edu

1359-6462/$ - see front matter © 2007 Acta Materialia Inc. Published by Elsevier Ltd. All rights reserved.
doi:10.1016/j.scriptamat.2007.04.049

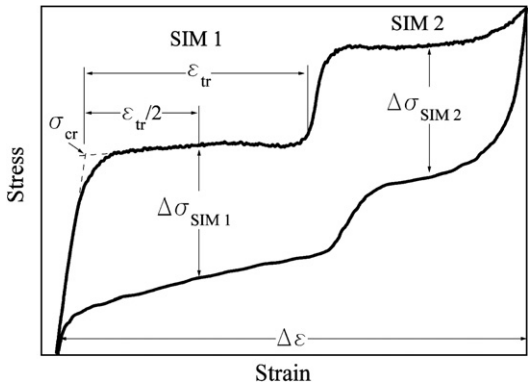

Figure 1. Schematic stress–strain curve defining the critical stress (σ_{cr}), the stress hysteresis ($\Delta\sigma$), the strain range ($\Delta\varepsilon$) and the transformation strain (ε_{tr}).

maximum strain [10,12,13,16]. In the case of a cyclically hardening material, fixed stress conditions produce a decrease in the applied strain and hence limit the fatigue damage. Similarly, constant maximum strain conditions limit fatigue damage when a material exhibits irreversible strain. The fixed strain range experiment represents the most demanding conditions for SMA fatigue studies.

Fatigue studies in SMAs fall into two categories: investigations of the deformation response and investigations of the fatigue lives. The majority of the literature reports on the first category, i.e. the deformation response and its degradation with cycles. We provide a brief review of both categories below.

Miyazaki et al. utilized a fixed strain range of 5% for the loading of polycrystalline NiTi [14]. The σ_{cr} and the $\Delta\sigma$ decreased 10–40% and stabilized after 100 cycles with a ratcheting strain of 0.25–0.75%. Sehitoglu and co-workers examined fixed strain range cycling to 3% in both tension and compression in NiTi single crystals [11]. They observed considerable cyclic hardening, ratchet strains of 0.6–0.9% and a decrease of σ_{cr} after 90 cycles. Sade and colleagues have also noted a decrease of approximately 33% in the σ_{cr} and a marked increase in the hardening slope for a fixed strain range of 5% in CuZnAl single crystals [9]. Kato et al. investigated constant maximum strain cycling to near 10% in CuAlMn [10]. They found changes up to 100% in the σ_{cr}, but significant ratchet strain (>8%) during the experiments resulted in almost purely elastic loading (elastic shakedown) by 1000 cycles. Strnadel and co-workers investigated differences between fixed stress ($R = 0$) and constant maximum strain cycling for polycrystalline NiTi and NiTiCu [13]. A constant maximum strain of 3% or a stress range of 1.1–1.2 σ_{cr} was utilized. For either test condition, decreases in σ_{cr} were near 50% of the initial values. Furthermore, both test conditions resulted in ratcheting strain (thus reducing the fatigue damage of each cycle). These results point to the need for fixed strain range control conditions to circumvent "elastic shakedown".

Fewer studies were conducted under the second category, which consists of investigating the fatigue lives. Melton and Mercier showed that fully reversed strain controlled cyclic experiments to ±5% strain resulted in a fatigue life of 1000 cycles for NiTi [1]. Miyazaki reported fatigue lives varying from 3000 to 30,000 for NiTi loaded to a constant maximum strain of 5% [16]. The range of fatigue lives varied depending on the heat treatment, and ratchet strains were below 1% (producing a strain range of 4%). In another study, Miyazaki and colleagues conducted rotating bending tests with a maximum surface strain of 3.5% on polycrystalline NiTi and NiTiCu wires; the corresponding lives were <10,000 cycles [8]. Sakamoto investigated the fatigue behavior of CuAlNi single crystals at 10% maximum strain and found fatigue lives of <3000 cycles [2]. In summary, the fatigue performance of SMAs are superior compared to conventional structural materials but there is a lack of fatigue information for strains of the order of 10%. The present investigation considers two categories: the stress–strain response during fixed strain range cycling, and the fatigue lives of NiFeGa.

The investigated alloy was cast to a nominal composition of $Ni_{54}Fe_{19}Ga_{27}$ (at.%). Single crystals were subsequently grown using the Bridgman technique in an inert environment. Small-scale dog-bone-shaped specimens with a 1.5×3 mm cross section and a 21 mm gauge length were electrodischarged machined with their loading axis along the [0 0 1], [0 1 1] or [1 2 3] crystallographic directions. Based on crystallographic considerations 8, 4 and 2 active correspondent variant pairs (CVPs) operate in the [0 0 1], [0 1 1] or [1 2 3] cases, respectively, with corresponding theoretical transformation strains of 14.5%, 4.1% and 7.1% for SIM1 + SIM2 [5]. The forward and reverse transformation temperatures (the peaks of the differential scanning calorimetry (DSC) curves) for this alloy were determined from DSC as 0 and 16 °C, respectively [3]. All the experiments were conducted at 25 °C, which is above the austenite reverse transformation temperature.

The σ_{cr} and the $\Delta\sigma$ of each first cycle, denoted by σ_1 and $\Delta\sigma_1$, respectively, were used to normalize subsequent cycles to study the stress–strain transients. This normalization also permits a comparison between the three orientations. The values of the elastic modulus and the σ_{cr} are based on an average of at least four measurements for each orientation. The elastic modulus was approximately 8 GPa for the [0 0 1], 30 GPa for the [0 1 1] and 40 GPa for the [1 2 3] orientation. The [0 0 1] orientation had a lower critical stress (64 MPa) compared to the [0 1 1] and [1 2 3] orientations (80 MPa). This was attributed to the greater resolved shear stress on the CVPs for the [0 0 1] orientation [5].

The fatigue response of the three orientations and the fatigue life, N_f (number of cycles to failure), are shown in Figure 2. Samples that did not fail are indicated by N_f = Runout. A comparatively short fatigue life of $N_f = 58$ was found for the [1 2 3] orientation when loaded to a 3% strain range (shown in Fig. 2a). At a smaller applied strain range of 1% the fatigue life was $N_f = 238$ and at 2% the fatigue life was $N_f = 117$ (not shown). The [0 1 1] orientation displayed a longer fatigue life ($N_f = 6427$) compared to the [1 2 3] orientation when loaded to a 1% strain range (Fig. 2b). None of the [0 0 1] specimens failed when loaded to strain ranges below 6%. Cycles greater than 18,000 were obtained at a 3% strain range without a significant change in the stress–strain

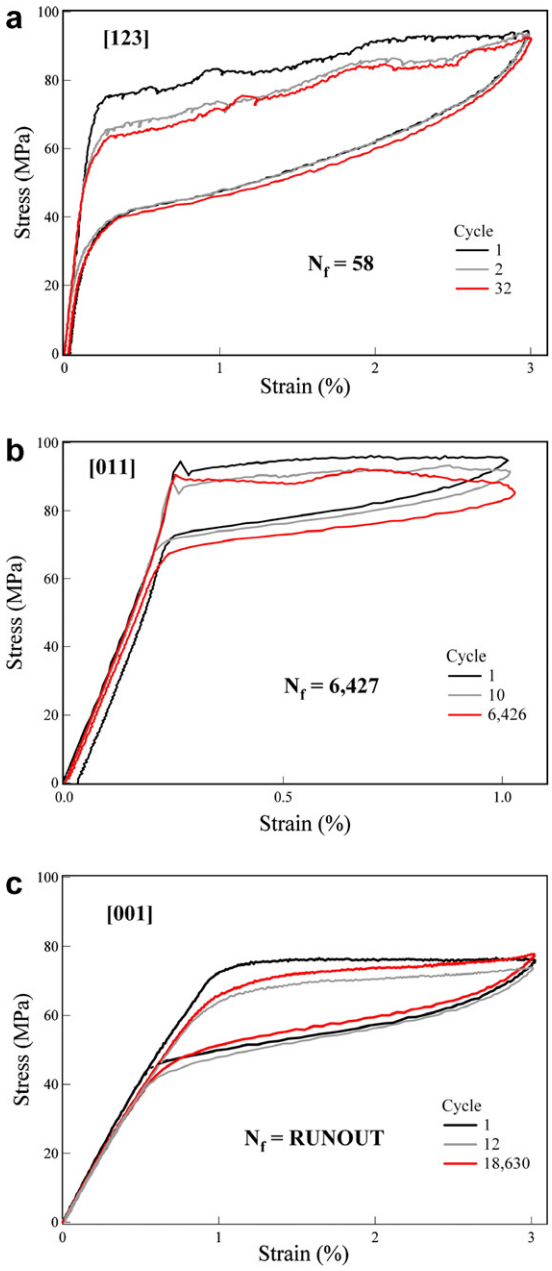

Figure 2. Cyclic pseudoelastic stress–strain curves: (a) [1 2 3], (b) [0 1 1], (c) [0 0 1].

response (Fig. 2c). All three orientations retained pseudoelastic response for the majority of their fatigue life (i.e. no ratcheting or residual strain). Additionally, the hardening slope remains stable during cycling for all orientations (Fig. 2).

Figure 3 shows the typical stress–strain behavior for the [0 0 1] orientation at a 10% strain range. At applied strain ranges >6%, the stress–strain curve displayed a two-stage transformation. This second transformation (SIM2) has a noticeable effect on the overall shape of the stress–strain curve, but the strain recoverability and the cyclic stability is retained. Although the specimen prematurely failed in the fillet section, a long fatigue life ($N_f = 13{,}579$) was found at a 10% strain range (Fig. 3). At an applied strain range of 12% the fatigue

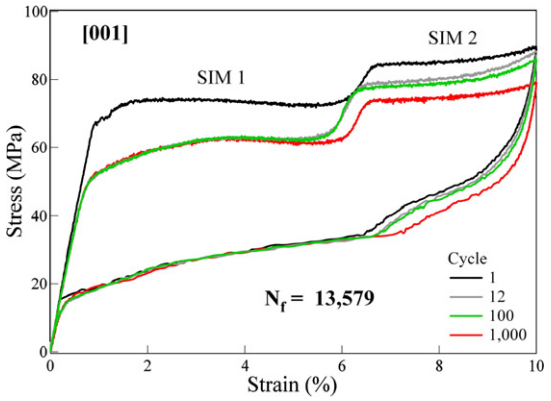

Figure 3. Cyclic stress–strain curve of the [0 0 1] orientation.

life was 558 cycles; again the failure was unavoidably at the fillet. These lives should be considered lower bounds because of failure at the fillet section.

The reduction of the σ_{cr} and $\Delta\sigma$ the for the [0 0 1] orientation is shown in Figure 4 for the 2, 3, 6, 10 and 12% strain ranges. The effect of cycling on the σ_{cr} was similar for strain ranges below 6% (indicated by the solid trend line) with a decrease of approximately 16%. The degradation of the σ_{cr} and $\Delta\sigma$ the for the [0 1 1] and [1 2 3] overlays the data shown in Figure 4 for strain ranges below 6% (not shown). The effect of cycling on the $\Delta\sigma$ was in the worst case approximately a 20% decrease for the [0 0 1] orientation and a 10% decrease for the [0 1 1] and [1 2 3] orientations. The σ_{cr} and the $\Delta\sigma$ became cyclically stable after 30 cycles, which is a small life fraction for most of the experiments considered. Also, minimal cyclic hardening was observed for all orientations and applied strains. This suggests that the effects of cycling are generated upon the initiation of the transformation not during the growth of the transformation to larger strains. However, above an applied strain range of 6%, the decrease in σ_{cr} occurred more rapidly and stabilized at approximately a 25% change (represented by the dotted black trend line). The effects of cycling on the $\Delta\sigma$ followed the same initial transient over a small life fraction of cycles and subsequently remained stable. The $\Delta\sigma$ did not seem to be

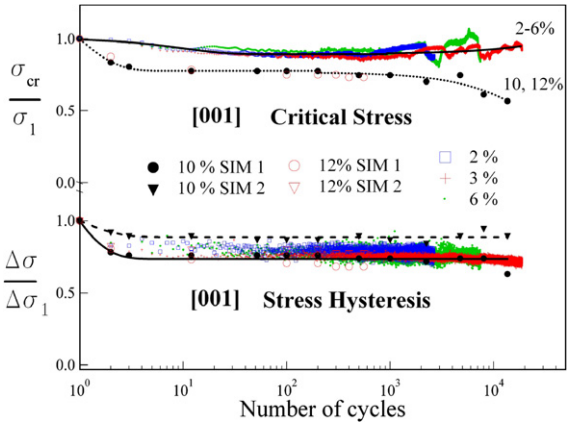

Figure 4. Change in the σ_{cr} and the $\Delta\sigma$ during cycling at the 2, 3, 6, 10 and 12% strain ranges.

affected by the applied strain range and decreased no more than approximately 20% until later in the fatigue life. Also note that $\Delta\sigma_{SIM2}$ (dashed black trend line) is as stable as $\Delta\sigma_{SIM1}$ (solid black trend line).

The experiments differed from most prior research where either a fixed stress or constant maximum strain was maintained. Since most previously investigated SMAs cyclically harden, maintaining fixed stress limits causes the deformation to decrease. Similarly, maximum strain endpoint-controlled tests would display a decreasing strain range as the material ratchets. On the other hand, the fixed strain range conditions utilized in this study maximize fatigue damage and allow a precise comparison of transients in the deformation response.

Complete pseudoelastic recovery was observed for nearly the entire duration of the experiments, ruling out the possibility of a high density of defect (dislocation) generation. The lack of changes in the cyclic loop shape and the lack of ratchet strain also suggests that cyclic loading does not produce significant dislocation emission or residual martensite as is commonly observed in other SMAs [11]. Irreversibilities such as residual martensite could interact with subsequently formed martensites and obstruct their expansion and growth. This would result in incomplete pseudoelasticity and hardening of the stress–strain slope [11]; however, this is not observed in NiFeGa.

Changes in the σ_{cr} and the $\Delta\sigma$ were $<16\%$ and 20%, respectively for strain ranges $<6\%$. These changes occurred over a small fraction of the life and the response was cyclically stable thereafter. Almost no cyclic hardening was observed in the three orientations investigated. The lack of cyclic hardening suggested minimal interaction between CVPs and or defects [9]. The degradation of the σ_{cr} for the [0 0 1] orientation was found to be dependent on the applied strain range above 6%. At strain ranges $>6\%$, the [0 0 1] orientation undergoes a two-stage transformation. Although the decrease in critical stress is affected by SIM2, the $\Delta\sigma$ is not altered. Furthermore, cycling through the two-stage transformation does not appear to decrease the fatigue life. The greater fatigue life for a given strain range in the [0 0 1] orientation could result from a combination of the larger number of active CVPs, the higher resolved shear stress factor and the lower initial modulus. Additionally, the [0 0 1] orientation is unfavorably oriented for slip [15].

In summary, this is the first time the fatigue resistance and the fatigue life have been investigated under a strain range of 12% in tension. Furthermore, to our knowledge, this is the first report on the fatigue life of NiFeGa, a very promising SMA. The lack of irreversible strains and the minimal degradation of the σ_{cr} and the $\Delta\sigma$ at strain ranges of 6–12% indicate excellent fatigue resistance.

The work was supported by a Grant CMS-0428428, the National Science Foundation, Division of Civil and Mechanical Systems and US–Italy Cooperative Research Program NSF OIS O4-37345.

[1] K.N. Melton, O. Mercier, Acta Metall. 27 (1979) 137.
[2] H. Sakamoto, Trans. J. Inst. Metals 24 (1983) 665.
[3] R.F. Hamilton, C. Efstathiou, H. Sehitoglu, Y.I. Chumlyakov, Scripta Mater. 543 (2006) 465.
[4] Y. Sutou, N. Kamiya, T. Omori, R. Kainuma, K. Ishida, K. Oikawa, Appl. Phys. Lett. 84 (2004) 1275.
[5] R.F. Hamilton, H. Sehitoglu, C. Efstathiou, H.J. Maier, Acta Mater., in press.
[6] K.N. Melton, O. Mercier, Mat. Sci. Eng. 40 (1979) 81.
[7] M. Thumann, E. Hornbogen, Z. Metallkd. 79 (1988) 119.
[8] S. Miyazaki, K. Mizukoshi, T. Ueki, T. Sakuma, Y. Liu, Mat. Sci. Eng. A 273 (1999) 658.
[9] M. Sade, R. Rapacioli, M. Ahlers, Acta Metall. 33 (1985) 487.
[10] H. Kato, T. Ozu, S. Hashimoto, S. Miura, Mat. Sci. Eng. A 264 (1999) 245.
[11] H. Sehitoglu, R. Anderson, I. Karaman, K. Gall, Y. Chumlyakov, Mat. Sci. Eng. A 314 (2001) 67.
[12] K. Gall, H.J. Maier, Acta Mater. 50 (2002) 4643.
[13] B. Strnadel, S. Ohashi, H. Ohtsuka, T. Ishihara, S. Miyazaki, Mat. Sci. Eng. A 202 (1995) 148.
[14] S. Miyazaki, T. Imai, Y. Igo, K. Otsuka, Metall. Trans. 17 A (1986) 115.
[15] H. Sehitoglu, J. Jun, X. Zhang, I. Karaman, Y. Chumlyakov, H.J. Maier, K. Gall, Acta Mater. 49 (2001) 3609.
[16] S. Miyazaki, in: T.W. Duerig, K.N. Melton, D. Stökel, C.M. Wayman (Eds.), Engineering Aspects of Shape Memory Alloys, Butterworth–Heinemann, London, 1990, p. 394.